Supplementary Information for

Cooperative subunit dynamics modulate p97 function

Rui Huang[1,2,3,4,*], Zev A. Ripstein[1,2], John L. Rubinstein[1,2,5], Lewis E. Kay[1,2,3,4,*]

[1]The Hospital for Sick Children, Program in Molecular Medicine, 555 University Avenue, Toronto, ON, Canada M5G 1X8

[2]Department of Biochemistry, University of Toronto, Toronto, ON, Canada M5S 1A8

[3]Department of Molecular Genetics, University of Toronto, Toronto, ON, Canada M5S 1A8

[4]Department of Chemistry, University of Toronto, Toronto, ON, Canada M5S 3H6

[5]Department of Medical Biophysics, University of Toronto, Toronto, ON, Canada M5G 1L7

Correspondence to

Rui Huang (ruihuangchem@gmail.com)
Lewis E. Kay (kay@pound.med.utoronto.ca)

This PDF file includes:

Supplementary text
Figs. S1 to S6
References for SI reference citations

www.pnas.org/cgi/doi/10.1073/pnas.1815495115

Supplementary Information Text

Cloning, protein expression and purification Full-length and ND1L (residues 1-480) p97 gene constructs from *Mus musculus* were generated with an N-terminal His_6-tag and a tobacco etch virus (TEV) cleavage site between the tag and the protein sequence (1, 2), unless specified otherwise. His_6-SUMO- and Strep-tagged p97 constructs were prepared using the NEB Gibson Assembly Master Mix via the Gibson assembly approach (3). Constructs with the His_6-SUMO-tag were sub-cloned into a pET vector with ampicillin resistance, with the remaining constructs sub-cloned into PET29b+ with kanamycin resistance. UBXD1N, comprising residues 1-133 of the full-length protein from *Mus musculus*, was prepared with an N-terminal His_6-tag and TEV cleavage site by expression of a gene sub-cloned into PET29b+. All proteins were expressed in Codon+ *Escherichia coli* BL21(DE3) cells. For unlabeled p97, transformed cells were grown in LB media, and protein expression was induced with 0.2 mM IPTG at OD_{600} = 0.7. To prepare p97 samples for NMR experiments, transformed cells were grown in minimal M9 D_2O media supplemented with $^{15}NH_4Cl$ and [^2H,^{12}C]-glucose as the sole nitrogen and carbon sources with addition of precursors (50 mg L^{-1} α-ketobutyrate, 100 mg L^{-1} $\varepsilon^{13}CH_3$ Met, and 230 mg L^{-1} 2-hydroxy-2-methyl-D_3-3-oxobutanoate-4-^{13}C for labeling Ileδ1-$^{13}CH_3$, Metε1-$^{13}CH_3$ and *proR*,Val/Leu-γ1/δ1-$^{13}CH_3$, respectively) 45 min prior to induction with 0.2 mM IPTG at OD_{600} = 0.8. Expression was allowed to proceed for *ca.* 18 hr at 18˚C. p97 and UBXD1N were purified as previously described (2).

Co-expression of WT- and R95G-ND1L and purification of hetero-hexamers Co-expression of WT His_6-SUMO-ND1L and R95G Strep-ND1L was achieved as follows: (i) Plasmids encoding WT His_6-SUMO-ND1L were transformed into *E. coli* BL21(DE3) cells; (ii) Transformed cells with ampicillin resistance were selected and made chemically competent; (iii) Plasmids encoding R95G Strep-ND1L were transformed into these cells; (iv) Cells with both ampicillin and kanamycin resistance were inoculated into LB media and protein expressed

according to the protocol described above. Purification was achieved by first passing the lysate through a StrepTactin affinity column in a buffer containing 50 mM Hepes (pH 7.5), 200 mM NaCl, and 1 mM EDTA, followed by elution with the same buffer but containing 2.5 mM desthiobiotin. After removal of desthiobiotin using a PD-10 desalting column (GE healthcare), the eluate was applied to a Ni affinity column to obtain hetero-hexamers comprised of both protomers. The Ni binding buffer contained 50 mM sodium phosphate (pH 7.5), 0.5 M NaCl, and 30 mM imidazole, while the elution buffer comprised 0.1 M sodium phosphate (pH 7.5) and 0.3 M imidazole. His_6-SUMO- and Strep-tags were subsequently cleaved using Ulp1 and TEV proteases, respectively, before the hetero-hexamers were re-submitted to Ni and StrepTactin columns as negative controls (*i.e.*, to ensure the absence of non-specific column binding).

Preparation of p97 hetero-hexamers *in vitro* To test for spontaneous formation of p97 hetero-hexamers via subunit exchange, purified His_6-SUMO-tagged WT and His_6-less (no tag) R95G ND1L (or full-length p97) homo-hexamers were mixed at various ratios and incubated at a total protomer concentration of 10 μM for 18 hr at 37 °C in a buffer containing 50 mM Hepes (pH 7.5), 200 mM NaCl, 1 mM EDTA and 1 mM DTT. After incubation His_6-containing and His_6-less hexamers were separated using a Ni affinity column, and the respective amounts of each were quantified by the absorbance at 280 nm under denaturing conditions.

To prepare hetero-hexamers comprised of randomly mixed protomers for NMR experiments and ATPase assays, we used a GdnCl-assisted unfolding-refolding protocol described previously (4). Purified homo-hexamers (*e.g.* WT and R95G) were mixed at a desired ratio, concentrated to 250 μL and added to an unfolding buffer containing 50 mM Hepes (pH 7.5), 200 mM NaCl, 10 mM DTT and 6M GdnCl to a final protomer concentration of 40 μM. The unfolded mixture was then refolded via 15-fold fast dilution into a refolding buffer containing 50 mM Hepes (pH 7.5), 200 mM NaCl, and 5 mM DTT. The solution was subsequently

concentrated and subjected to a HiLoad 16/60 Superdex 200 gel filtration column to obtain refolded hetero-hexamers.

ATPase assays ATPase activities of hetero-hexamers comprised of WT and R95G (E305A) ND1L protomers were measured using a NADH-coupled assay that has been previously described (5, 6). The reaction was carried out with a total protomer concentration of 27 μM and an ATP-regeneration system that contained 2.5 mM phosphoenolpyruvate, 0.2 mM NADH, 50 μg/mL pyruvate kinase, 50 μg/mL lactate dehydrogenase, and 3 mM ATP in a buffer comprising 25 mM Hepes (pH 7.5), 50 mM NaCl and 20 mM $MgCl_2$. The reactions were monitored with a SpectraMax i3X Microplate Reader by the change of the absorbance at 340 nm at 25 °C for 30 min. All measurements were performed in triplicate.

NMR sample preparation Prior to NMR experiments, protein samples were exchanged into the NMR buffer containing 25 mM Hepes (pH 7.0), 50 mM sodium chloride, 3mM TCEP and 99.9% D_2O using a centrifugal concentrator (50-kDa molecular mass cutoff). For p97-ADP, a final concentration of 5 mM ADP was added into the sample after buffer exchange. To obtain apo-p97, the sample was treated with apyrase (New England Biolabs; 5 units per mM of protomers) for *ca.* 16 hr at 25 °C, followed by size exclusion chromatography on a HiLoad 16/60 Superdex 200 gel filtration column to remove apyrase and exchanged into the NMR buffer. NMR samples were prepared with a total protomer concentration of 150-200 μM for homo-hexamers and 250-400 μM for hetero-hexamers.

Hetero-hexamers comprising U-^{2}H, I-$^{13}CH_3$ labeled WT and cross-linked U-^{2}H, *proR*,LV labeled R155C+N387C (apo state) were prepared as follows: (i) Cross-linking by leaving the hetero-hexamers in non-reducing buffer containing 5 mM ADP for 2 days at 4 °C (the progress of cross-linking was monitored by NMR); (ii) Removing ADP using a PD-10 desalting column (GE healthcare) followed by apyrase digestion described above; (iii) Removal of apyrase and

exchange to NMR buffer. 5 mM DTT was added later to the same sample to obtain the reduced apo form.

Electron cryo-microscopy To prepare samples for electron cryo microscopy (cryo-EM), full-length R95G was treated with apyrase as described above and purified using a Superdex 200 gel filtration chromatography column. Fractions corresponding to the p97 peak were concentrated to ~15 mg/mL in a buffer comprising 50 mM Hepes (pH 7.5), 200 mM NaCl, 1mM $MgCl_2$, and 5 mM TCEP. Following concentration the complex was incubated with 10 mM ADP and immediately before freezing 0.025 % (wt/vol) IGEPAL CA-630 (Sigma-Aldrich) was added to increase the number of particles adopting side-views on the grid. A total of 2.5 μL of sample was applied to nanofabricated holey sputtered gold grids (7, 8) with a hole size of ~1 μm, and blotted using a modified FEI Vitribot for 4.5 s before plunge freezing in a liquid ethane/propane mixture (ratio of ~3:2) held at liquid nitrogen temperature.

Movies consisting of 30 frames over a 60 second exposure were collected with defocuses ranging from 1.0 to 3.9 μm using a FEI Titan Krios G3 operating at 300kV and equipped with a FEI Falcon 3EC DDD camera. Movies were collected in counting mode at a nominal magnification of 75000 × corresponding to a calibrated pixel size of 1.06 Å and with an exposure rate of 0.8 electrons/pixel/s, giving a total exposure of 43 electrons/$Å^2$. 2796 movies were collected semi-automatically using EPU software.

EM Image Processing Whole frame alignment was performed with an implementation of *alignframes_lmbfgs* (9) in the *cryoSPARC* v2 package (10) and the resulting averages of frames were used for contrast transfer function determination with CTFFIND4 (11) and automated particle selection with RELION (12). Particle coordinates were used to extract particles in 256-pixel boxes from the aligned movies, while performing individual particle alignment and exposure weighting with a reimplementation of *alignparts_lmbfgs* (9) *cryoSPARC* v2. The R95G dataset of 757274 particle images was initially cleaned with two rounds of 2D classification,

followed by *ab initio* reconstruction with a single class yielding the familiar hexameric ring. Refinement of this class of 340735 particle images with C6 symmetry led to a map at 3.7 Å as determined by gold standard Fourier shell correlation (gsFSC). The density for the NTDs was highly fragmented in this reconstruction. Using this refined map as reference, 3D classification was performed as shown schematically in Figure S1, leading ultimately to 20 maps with varying arrangements of NTDs in *up* or *down* states.

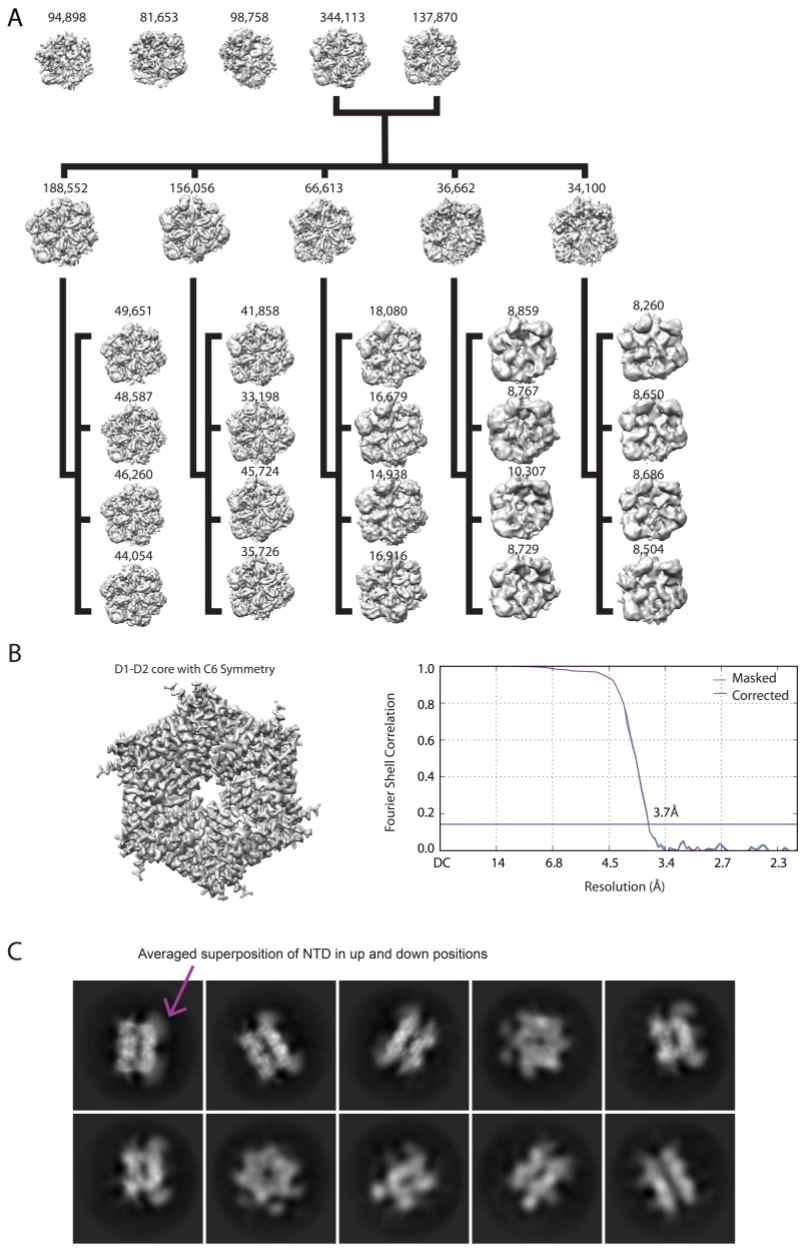

Fig. S1. Electron cryo-microscopy of R95G hexamers. (A) Classification scheme for identifying sub-populations of hexamers with mixtures of NTDs in the *up* and *down* conformations. In the first round of classification, two classes showed high-resolution features and were carried forward for further analysis. The subsequent two rounds of classification revealed multiple species, however many of those still contained NTD positions that were indeterminate mixtures of *up* and *down*. Number of particle images belonging to each class is indicated above the structure. (B)

Refinement of structure with C6 symmetry led to a reconstruction at 3.7 Å, with the D1-D2 core of the complex well resolved. However, applying symmetry led to fragmented densities for the NTDs. (C) Representative 2D classes of the R95G hexamers. A typical view shows the blurring of the NTDs compared to D1-D2 due to averaging of the *up* and *down* conformations.

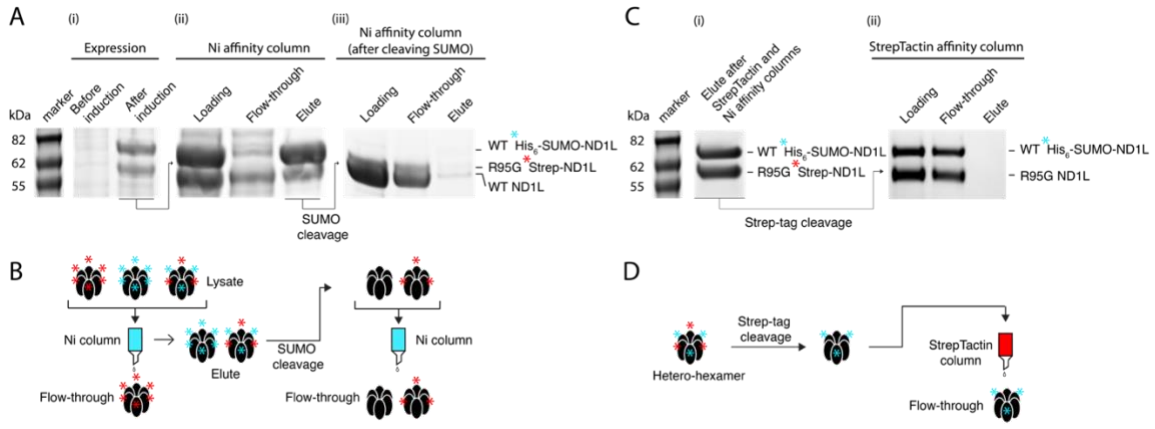

Fig. S2. Non-specific binding of hexamers to affinity columns does not occur. (A) Co-expression (i) of His_6-SUMO(blue star)-WT and Strep(red star)-R95G ND1L constructs results in mixed hexamers (*i.e.*, comprised of both types of subunits) as indicated by the presence of R95G Strep-ND1L in the elute fraction from the Ni affinity column (ii). Cleavage of the SUMO-tag eliminates binding of both subunits to the Ni column (iii), ruling out the possibility of non-specific binding. The procedure is described in (B). Similarly, cleavage of the Strep-tag from hetero-hexamers that are purified from both StrepTactin and Ni affinity columns (C, i) prevents subsequent binding to the StrepTactin column (C, ii), as described by the schematic in (D). Thus, the bands observed in Figure 2A(ii, Elute), Figure 2C(Elute), and Figure 2E(Elute) establish that mixing of subunits has occurred, as opposed to non-specific binding of hexamers to either the Ni affinity or StrepTactin columns.

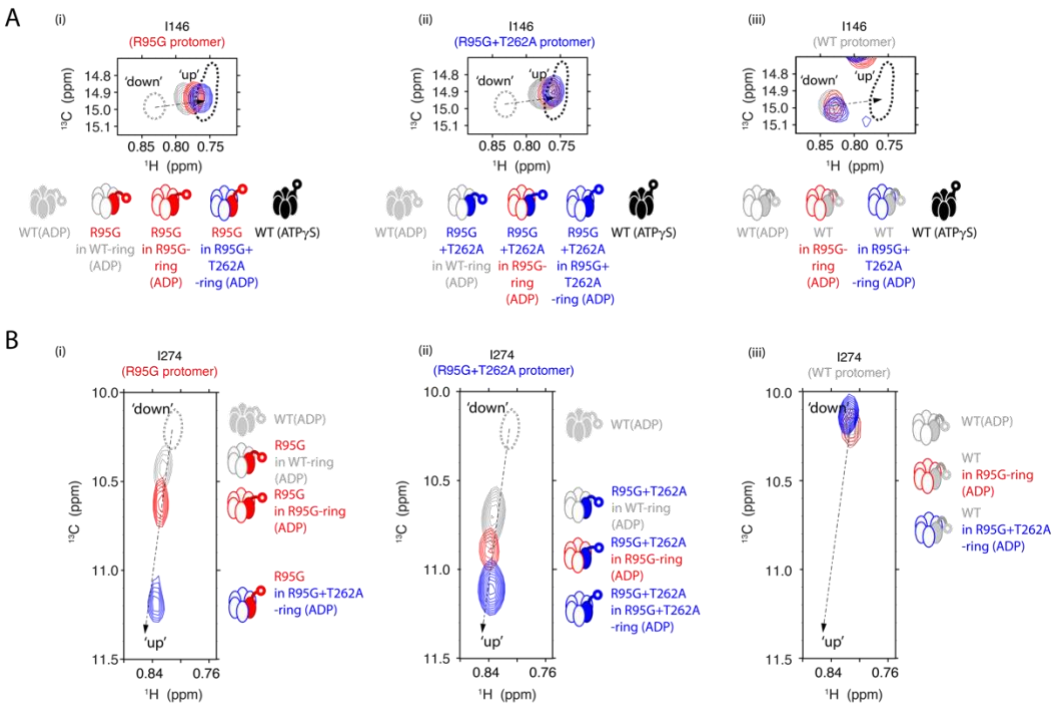

Fig. S3. Cooperative *up/down* NTD equilibrium, as established by I146 and I274 methyl probes. Superposition of selective regions from ^{13}C-^{1}H HMQC spectra (18.8 T, 50 °C) focusing on Ileδ1 methyl correlations from I146 (A) and I274 (B) recorded on hetero-hexamers comprised of 15% U-^{2}H, I-$^{13}CH_3$ (NMR visible, filled ovals) and 85% U-^{2}H (NMR invisible, empty ovals) protomers, prepared via GdnCl unfolding/refolding. Schematics of the hetero-hexamers are shown at the bottom (A) and to the right of the panels (B) with WT(ADP), WT(ATPγS), R95G and R95G+T262A protomers colored in grey, black, red, and blue, respectively. R95G, R95G+T262A and WT protomers are NMR visible in (i), (ii) and (iii), respectively, and peaks are colored according to the NMR invisible protomers in the ring. Only a single NTD, that of the NMR visible protomer, is highlighted. Peak positions in ADP- and ATPγS-loaded U-^{2}H, I-$^{13}CH_3$ WT ND1L are indicated by the dashed grey and dashed black single contours, respectively. Note that the I274 peak for ATPγS-loaded WT ND1L is not shown due to the proximity of I274 to the nucleotide which subsequently influences its spectral position.

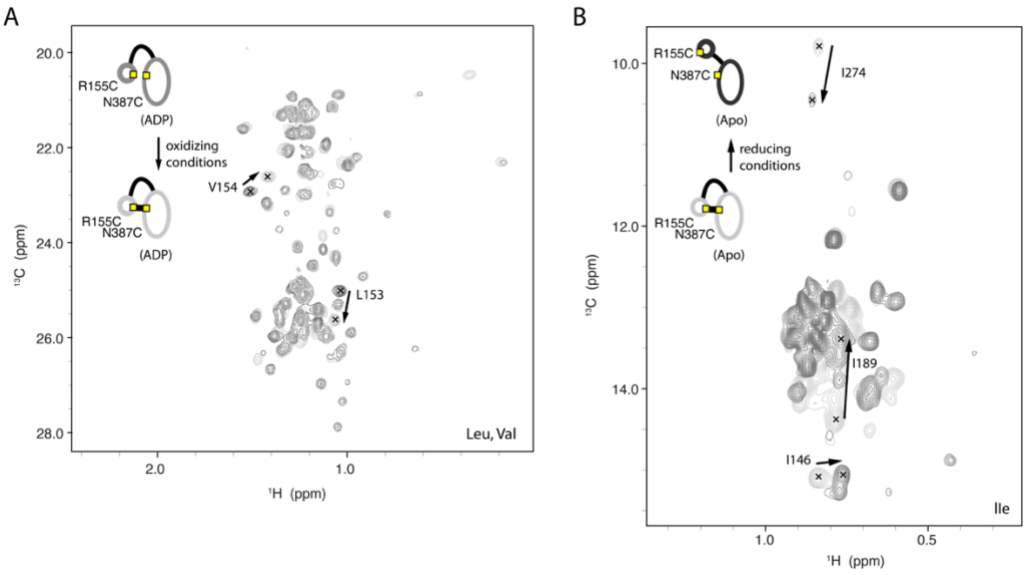

Fig. S4. Formation of C155-C387 disulfide can be controlled by oxidizing/reducing conditions. (A) Formation of disulfide bond between proximal C155 and C387 residues (yellow squares) in R155C+N387C ND1L bound to ADP is indicated by chemical shift perturbations of residues Leu153 and Val154, which are located in the vicinity of the disulfide bond; peaks in dark and light grey correspond to before and after oxidization, respectively. (B) Reduction of the C155-C387 disulfide bond in the apo state 'unlocks' the NTD and results in a significant shift of the NTD equilibrium from an all-*down* state (light grey) to a partially *up* state (dark grey), as evidenced by shifts in peak positions of Ile146, Ile189 and Ile274 that report on the *up/down* equilibrium (indicated by arrows).

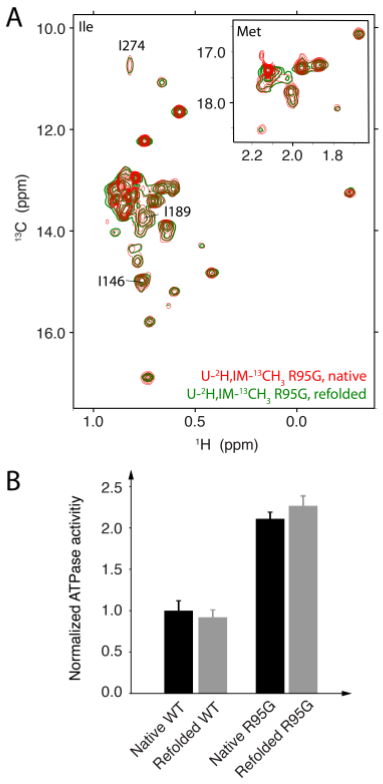

Fig. S5. GdnCl unfolding and refolding has no effect on the structure or ATPase activity of p97 ND1L. (A) Superposition of the Ile and Met (inset) regions from ^{13}C-^{1}H HMQC spectra (18.8 T, 50 °C) of native (red) and refolded (green) U-^{2}H, I-^{13}CH$_3$ labeled R95G ND1L homo-hexamers. The overall structure is not affected by the unfolding-refolding procedure, as evidenced by the superposition of the spectra. I146δ1, I189δ1and I274δ1 cross-peaks are highlighted to show that the NTD *up/down* equilibrium is also preserved. (B) ATPase activities of the native and refolded WT and R95G ND1L homo-hexamers, indicating no change in the ATPase activity due to refolding.

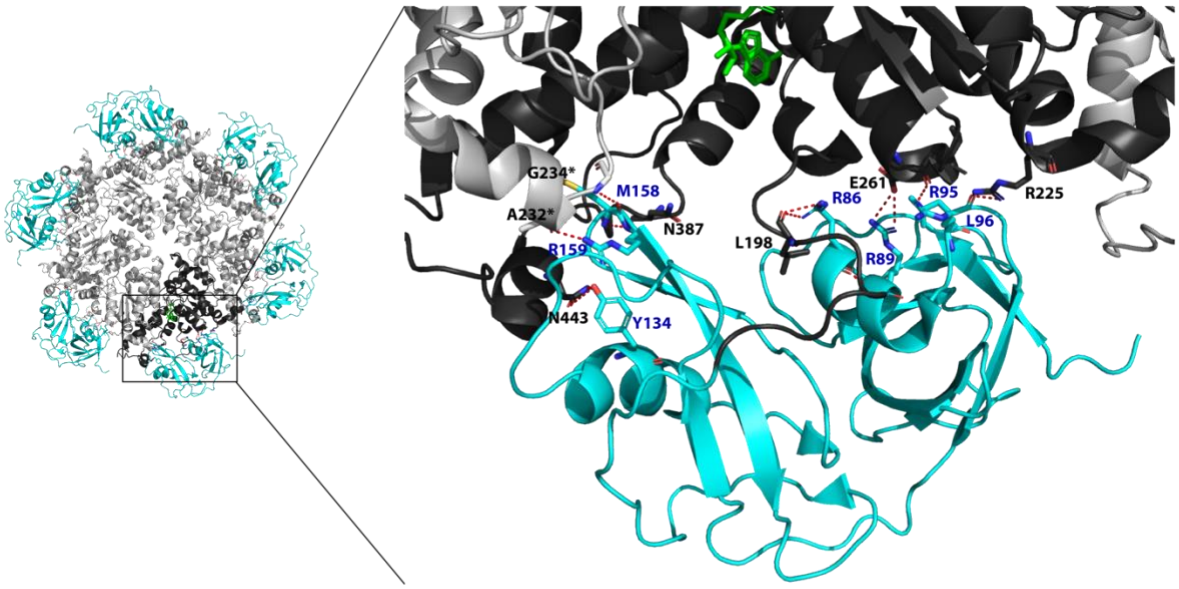

Fig. S6. Extensive intra- and inter-protomer hydrogen-bond network connecting NTD and D1 domains in the *down* state. Top view of p97 in the ADP state (PDB ID code 5FTK) with the NTDs colored cyan, D1 in black or grey, and D2 not shown (left). The NTD-D1 interface for one of the protomers is enlarged (right) to show the hydrogen bonds (red dashed lines) between residues on the NTD (blue sticks) and D1 domains of the same (black sticks) or the neighboring protomer (grey sticks, asterisks). Hydrogen bonds are formed in the vicinity of both inter-protomer interfaces (*i.e.*, from each side), suggesting potential pathways of communication between neighboring subunits.

References

1. Schütz AK, Rennella E, Kay LE (2017) Exploiting conformational plasticity in the AAA+ protein VCP/p97 to modify function. *Proc Natl Acad Sci* 114(33):E6822-6829.
2. Schuetz AK, Kay LE (2016) A dynamic molecular basis for malfunction in disease mutants of p97/VCP. *Elife* 5:e20143.
3. Gibson DG, et al. (2009) Enzymatic assembly of DNA molecules up to several hundred kilobases. *Nat Methods* 6(5):343–345.
4. Huang R, Pérez F, Kay LE (2017) Probing the cooperativity of Thermoplasma acidophilum proteasome core particle gating by NMR spectroscopy. *Proc Natl Acad Sci* 114(46):E9846–E9854.
5. Nørby JG (1988) Coupled assay of Na+,K+-ATPase activity. *Methods Enzymol* 156:116–119.
6. Huang R, et al. (2016) Unfolding the mechanism of the AAA+ unfoldase VAT by a combined cryo-EM, solution NMR study. *Proc Natl Acad Sci U S A* 113(29):E4190–E4199.
7. Marr CR, Benlekbir S, Rubinstein JL (2014) Fabrication of carbon films with ~500nm holes for cryo-EM with a direct detector device. *J Struct Biol* 185(1):42–47.
8. Russo CJ, Passmore LA (2014) Ultrastable gold substrates for electron cryomicroscopy. *Science* 346(6215):1377–1380.
9. Rubinstein JL, Brubaker MA (2015) Alignment of cryo-EM movies of individual particles by optimization of image translations. *J Struct Biol* 192(2):188–195.
10. Punjani A, Rubinstein JL, Fleet DJ, Brubaker MA (2017) cryoSPARC: algorithms for rapid unsupervised cryo-EM structure determination. *Nat Methods* 14(3):290–296.
11. Rohou A, Grigorieff N (2015) CTFFIND4: Fast and accurate defocus estimation from electron micrographs. *J Struct Biol* 192(2):216–221.
12. Scheres SHW (2015) Semi-automated selection of cryo-EM particles in RELION-1.3. *J Struct Biol* 189(2):114–122.